Optics Letters

Coherent multi-band MIMO radar: robustness analysis to SSMF-based RF signal delivery

Gaurav Pandey,[1,*] Mirco Scaffardi,[2] Salvatore Maresca,[3] Malik Muhammad Haris Amir,[1] Antonella Bogoni,[1,2] and Antonio Malacarne[2]

[1]Sant'Anna School of Advanced Studies, Institute of Technologies of Communications, Information, and Perception, 56124 Pisa, Italy
[2]National Inter-University Consortium for Telecommunications (CNIT), Photonic Network and Technology Lab, 56124 Pisa, Italy
[3]National Research Council (CNR), Institute of Electronics, Information Engineering and Telecommunications, 56124 Pisa, Italy
*gaurav.pandey@santannapisa.it

Received 25 October 2023; revised 2 February 2024; accepted 9 February 2024; posted 13 February 2024; published 11 March 2024

A numerical evaluation is conducted to assess the impact of distributing radio frequency (RF) signals through optical fiber links on the performance of a coherent multi-band multiple-input multiple-output (MIMO) radar system. The analysis focuses on scenarios where the antennas are widely separated in comparison to the employed signal wavelengths. The development of a model to quantify the phase noise (PN) induced on each RF band due to the signal transmission through optical fiber links between the centralized base station and each radar peripheral is described. Monte Carlo simulation results are collected to estimate the key performance indicators (KPIs) for varying standard single-mode fiber (SSMF) length and different PN contributions. The main contributors to the PN are revealed to be chromatic dispersion (CD), double Rayleigh scattering (DRS), and mechanical vibrations. In a shipborne scenario, a significant performance degradation occurs only when the length of the fiber links reaches approximately 20 km. Further, the PN impact has also been studied in a shipborne scenario to analyze the robustness of the system for worse phase noise level assumptions. The results reveal excellent robustness of the proposed centralized acquisition and processing approach in the presence of both very long fiber links and economically employed RF oscillators.

https://doi.org/10.1364/OL.510328

Multiple-input multiple-output (MIMO) radars with widely separated antennas offer significant advantages due to their geometric diversity gain, allowing to address the matters arising from radar cross section (RCS) fluctuations and slow-moving target detection [1]. These benefits translate into improved performance for target detection and parameter estimation, such as target location [1] and velocity [2]. Moreover, additional diversity domains, such as frequency diversity, can be explored by operating radar peripherals (RPs) on multiple RF bands [3].

In *coherent* MIMO radars, the phase coherence among all received signals is crucial to enhance the spatial resolution beyond the limit imposed by the total bandwidth and make it comparable to the employed wavelength [4]. However, such advantage comes at the cost of increased system complexity, demanding precise time and phase synchronization among the RPs and requiring long and wideband RF links.

Nevertheless, microwave photonic (MWP) techniques have emerged as a promising solution to address these challenges. Long RF links can be implemented through optical fiber transmission [5,6], and the coherence among multiple bands within a radar network can be kept through photonics-based up- and downconversion [7]. Notably, experimental outdoor demonstrations of MWP-based radar systems [8], which incorporate multi-band and widely separated antennas [6], have been successfully carried out. These advancements in MWP technology pave the way for more efficient and capable radars in the near future. Here a photonics-based coherent multi-band MIMO radar architecture is considered. The focus is on modeling the phase noise (PN) that arises from distributing RF signals through a standard single-mode fiber (SSMF). The impact of such PN has been examined using relevant key performance indicators (KPIs) [9]. The analysis is conducted for a shipborne scenario, where fiber links span 100s of meters.

Figure 1 illustrates the architecture of the proposed photonics-based coherent multi-band MIMO radar system. The architecture employs a central unit (CU) to generate multiple radar signals (three in this instance), such as frequency-modulated continuous waves (linear chirp), each at a distinct intermediate frequency (IF): f_{IF1}, f_{IF2}, and f_{IF3}, as depicted in Fig. 1. At the same time, an optical frequency comb (OFC) is generated with mode spacing f_{comb}, achieved through opto-electronic modulation driven by an electronic local oscillator (LO) operating at frequency f_{comb}. The OFC is then modulated using an opto-electronic Mach–Zehnder modulator (MZM) driven by the sum of the IF radar signals. Both the modulated and unmodulated versions of the OFC are transmitted through optical fiber links to multiple RPs. Each RP has the capability to transmit and receive signals at each RF band using appropriate front ends.

To distinguish the corresponding RP transmitter for each received echo, time division multiplexing (TDM) is employed. At each RP, the modulated and unmodulated OFC signals are separated (e.g., through spatial separation with distinct fibers, utilizing polarization diversity or wavelength diversity). The modulated version of the OFC enters a photodetector (PD), resulting in the generation of the upconverted multi-band radar

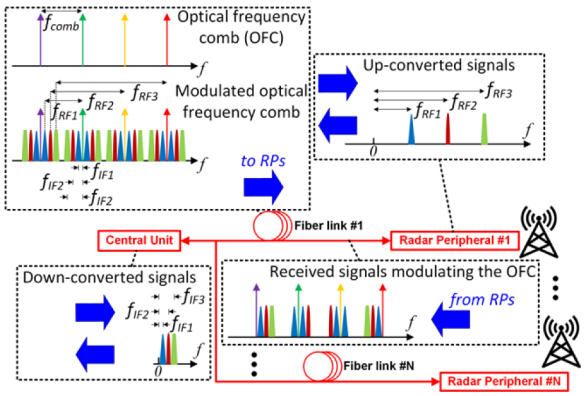

Fig. 1. Schematic of the photonics-based coherent multi-band MIMO radar system showing the signal distribution among the central unit and radar peripherals through optical fiber links.

signal. Notably, each f_{IF} is upconverted to a distinct f_{RF}, as illustrated in Fig. 1. At each RP, the unmodulated version of the OFC is modulated once again through an opto-electronic MZM, driven by the backreflected echoes. This modulated OFC version is then sent back through the SSMF link to the CU. Here, another PD (one for each RP) generates multiple beating terms, including those at the original intermediate frequencies. These downconverted signals are subsequently digitized and processed centrally in a coherent manner.

The exceptional performance offered by the coherent MIMO processing strategy relies heavily on maintaining a high degree of phase coherence among the received echo signals. Referring to the architecture depicted in Fig. 1, such phase coherence may be significantly influenced by various sources of PN that occur during the optical fiber transmission of the signals. These sources of PN are thermodynamic fluctuations, amplitude-to-phase noise conversion, double Rayleigh scattering (DRS), and mechanical vibrations.

Thermodynamic fluctuations in the fiber induce changes in its refractive index and physical length, resulting in group delay variations that lead to PN [10]. The power spectral density (PSD) of this PN term on each RF carrier is derived in [11] and is directly proportional to the fiber length L and the square of the generated radio frequency f_{RF}.

Amplitude-to-phase modulation (AM-PM) conversion in the PD or in other microwave components also contributes to PN [12]. However, the resulting term has no explicit dependence on L and f_{RF} and turns out to be negligible [10].

The group velocity of light in the fiber is influenced by its optical frequency, leading to chromatic dispersion (CD). Consequently, the signal group delay varies due to the frequency noise of the laser, resulting in microwave PN [13]. This PN term can be expressed as [10]

$$\mathcal{L}_{CD}(\omega) = \frac{1}{2}\left(\frac{\omega_{\mathrm{RF}}\lambda^2 D_\lambda}{c}\right)^2 L^2 S_{\vartheta,\mathrm{laser}}(\omega), \tag{1}$$

where λ is the laser wavelength, D_λ is the fiber dispersion coefficient, $S_{\vartheta,\mathrm{laser}}(\omega)$ is the PSD of the laser frequency noise, and $S_{\vartheta,\mathrm{laser}}(f) = f^2 \times S_{\phi,L}(f)$ where $S_{\phi,L}(f)$ is the PSD of the laser PN. Hence, the CD-induced microwave PN is directly proportional to L^2 and to the square of $\omega_{RF} = 2\pi f_{RF}$.

Microscopic variations in material density along the fiber lead to Rayleigh scattering, where a portion of light scatters at an angle of ~180°, traveling in the opposite direction to the incident light. Some of the reflected light is then reflected back, causing interference with the original incident light and inducing optical RIN, which in turn leads to microwave PN [14]. The DRS-induced microwave PN exhibits super-linear growth below a certain fiber length and in certain detuning frequency ranges. Beyond that value, the PN grows linearly or sub-linearly, depending on the magnitude of the laser PN, which determines the transition between these regimes [15]. The DRS-induced microwave PN is independent of the microwave frequency, and its analytical expression can be found in [14]. A negligible impact on the system performance results from the higher-order Rayleigh scattering, and thus, it has not been considered.

In [10], the various noise contributions have been evaluated concerning the detuning frequency from f_{RF}, assuming a quiet, underground fiber installation with no mechanical vibrations. The primary contributors to the PN are identified as DRS and CD, while other phenomena are considered negligible. The overall PSD of the PN resulting from the transmission over a given SSMF length L and at a specific f_{RF} has been approximated as follows:

$$\mathcal{L}(L, f_{\mathrm{RF}}) = 10 \times log_{10}(PN \cdot L^2 \cdot f_{\mathrm{RF}}^2)\,[\mathrm{dBc/Hz}], \tag{2}$$

where PN is the PN PSD per fiber length unit and frequency unit, extrapolated from the experimental curves in [10]. Equation (2) represents an overestimation, as here the PN PSD scales with the square of both L and f_{RF} whereas the DRS, as previously explained, only scales with L.

In scenarios where optical fibers are used for distributing radar signals in terrestrial, maritime, or air vehicles, mechanical vibrations become significant, especially in situations involving engines, rough terrain, sea waves, and air turbulence. These vibrations contribute to phase fluctuations in the transmitted signal propagating through the fiber, particularly at low detuning frequencies ranging from 1 Hz to 10 kHz. In shipborne coherent MIMO radars, these fiber vibration-induced phase fluctuations can impact the KPIs of the radar system. Vibrations are commonly measured as acceleration [16], and the relationship between mechanical vibrations and their impact on microwave signal PN are analyzed in [17], considering different types of fiber.

To assess the total PN, DRS and CD contributions are calculated using Eq. (2). The additional term due to mechanical vibrations is obtained from the experimental data under a specific acceleration coefficient [17] and scaled according to shipborne scenario vibrations [16] assuming a direct proportionality. By extrapolating the results from [17] and considering relevant accelerations for an actual vessel scenario (40 m/s^2) [16], the effect of vibrations on the phase fluctuations of the transmitted signal in a shipborne coherent multi-band MIMO radar is assessed. The total extrapolated PN PSD for a vessel, eventually included in Eq. (2), is shown in Fig. 2, where the impact of vibrations is evident from 1 Hz to 10 kHz. Additionally, at higher detuning frequencies, the effects of DRS and CD are highlighted. For detuning frequencies above 1 MHz, a typical flicker noise decay assumption is made.

Ambiguity function-related KPIs were assessed through MATLAB simulations for a coherent multi-band MIMO radar. In the considered shipborne scenario, the RPs are positioned with a wide separation along a 100-meter linear baseline. The RPs comprise two transmitters and four receivers, with transmitter (TX) coordinates at −50 m, +25 m, and receiver (RX)

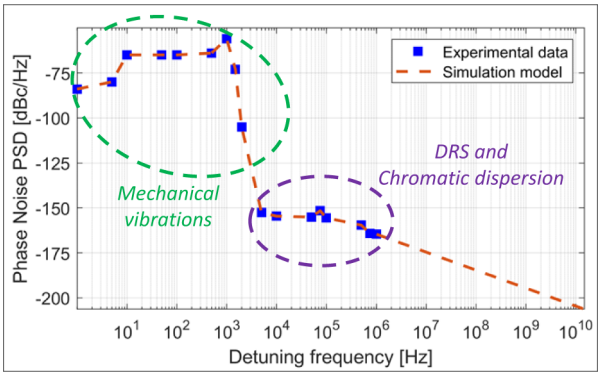

Fig. 2. Extrapolated PN PSD when vibrations effects are considered (curve obtained for $f_{RF} = 10$ GHz, 1 km SMF).

coordinates at −25, −10, +10, and +50 m. Each TX and RX operates at three RF bands (8/9/10 GHz), each with a bandwidth of 600 MHz, resulting in a total of 24 virtual channels. The PN between different bands and the TX/RX components are mutually independent, thus considering the most unfavorable condition. The TDM strategy is employed to distinguish the transmitters. The radar signals between the base station and each RP are assumed to be transmitted via the SSMF, and the impact of various fiber lengths is analyzed. The evaluated KPIs for a point-like scatterer at a distance of 1200 m include the range resolution, cross-range resolution, peak-to-average sidelobe ratio (PASR), peak-to-maximum sidelobe ratio (PMSR), and target localization accuracy [9]. A 10 m × 10 m monitored area with spatial resolution of 1 cm was considered. To model the PN accurately at very low detuning frequencies, a long pulse train is simulated to achieve millisecond-level integration time. The simulation involves generating 100 ns-long pulses with a 10 µs pulse repetition interval, resulting in a total pulse train time duration of 10 ms. Realistic additive white Gaussian noise and signal-to-noise (SNR) evolution are considered on each received signal, accounting for both the SNR of generated signals and receiver noise, as well as the scaling of the receiver noise with the received signal power, dependent on the target distance. Monte Carlo simulations are performed showing both the mean value and distribution variance of the calculated parameter for each considered fiber length. From Fig. 3, it is evident that significant degradation in the range and cross-range resolution only occurs for fiber lengths exceeding 25 km. Correct target localization is achieved up to a fiber length of 25 km. However, PASR and PMSR notably decrease for fiber lengths beyond 10 and 20 km, respectively. In Fig. 4, the calculated coherent MIMO ambiguity function (AF) illustrates the PN impact in cases of 5, 20, and 30 km-long fiber links. As a consequence of the analysis revealed in Fig. 3, for very long fiber length, high sidelobes appear, and the mainlobe gets distorted and wider in both the range and cross-range. Please refer to [5] for the detailed calculation of the coherent MIMO AF.

The robustness of the system performance has been then assessed for increasing PN levels, mimicking a lower-quality RF LO. In particular, a variable vertical shift of the PN plot of Fig. 2, keeping the descending flicker noise behavior for high detuning frequencies and assuming a constant floor for detuning frequency ≥10 kHz, has been evaluated for both, considering 200 m SSMF links in the same shipborne scenario. In the latter case a PN floor for detuning frequencies ≥10 kHz can be the

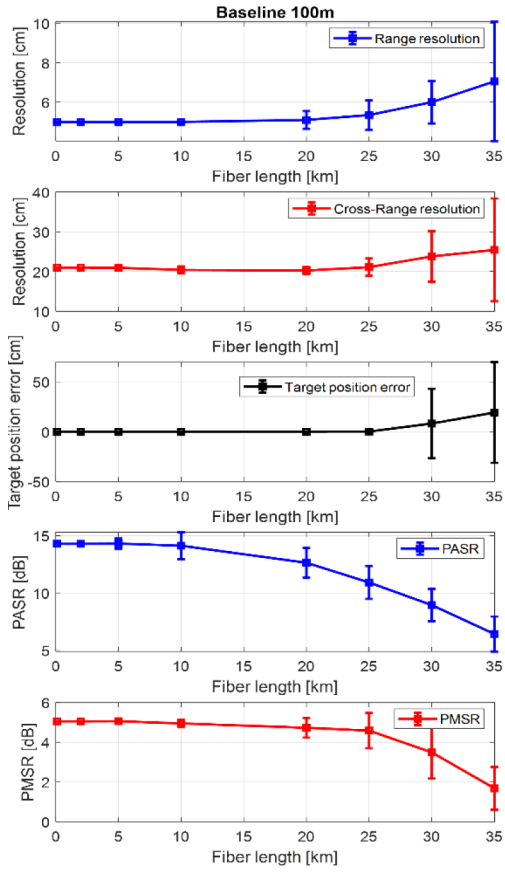

Fig. 3. KPI evolution in a tri-band 2 × 4 MIMO radar with 100-meter baseline and RF frequencies of 8/9/10 GHz. Monte Carlo simulation analyzes the fiber-induced PN with varying lengths, revealing mean values and distribution variance.

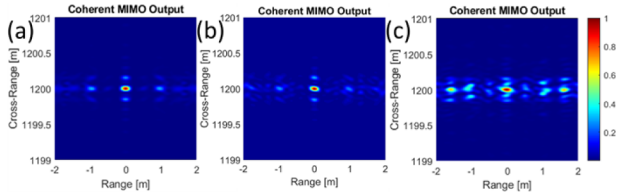

Fig. 4. Coherent MIMO ambiguity function for 8/9/10 GHz carrier frequencies and 5 km- (a), 20 km- (b), and 30 km-long (c) fiber link.

result of a limited SNR due to low-quality electrical chains in the system hardware. The PN caused by mechanical vibrations remains constant, while for the detuning frequency ≥10 kHz, it is altered. Monte Carlo simulations are conducted for different floor values. The analysis shown in Fig. 5 for the flat PN floor reveals significant degradation in the range and target position error beyond −100 dBc/Hz PN level, as well as concerning the PASR and PMSR. In the case of the descending flicker noise (higher SNR of received signals), the overall performance clearly improves showing robustness up to a PN level of about −70 dBc/Hz. Based on those results, the study confirms the suitability of using commercial X-band oscillators [18] and conventional electric devices for the proposed coherent multi-band MIMO radar approach.

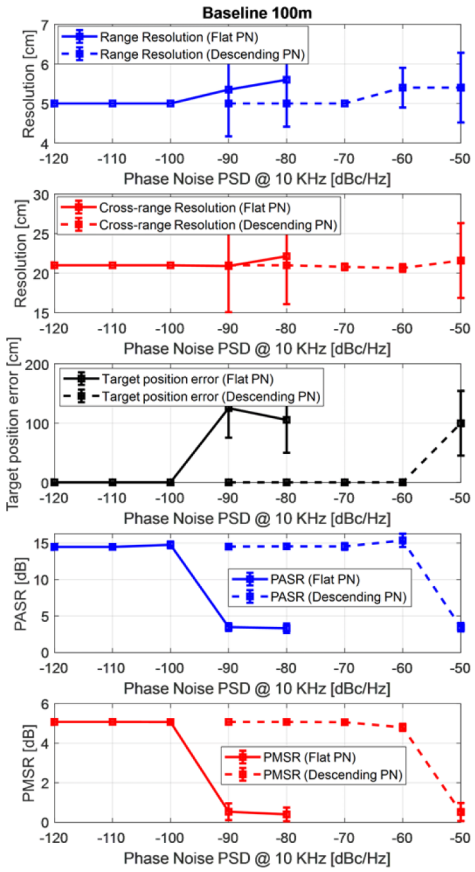

Fig. 5. KPI evolution in a tri-band 2×4 MIMO radar with 100-m baseline and RF frequencies of 8, 9, and 10 GHz for different PN.

In conclusion, Monte Carlo simulations have been used to test the performance potential of a photonics-based coherent multi-band MIMO radar with widely separated antennas, in the case of the RF signal distribution through optical fiber links between a centralized unit and each radar peripheral. A model for the PN induced by fiber transmission on each RF band was developed. In the considered shipborne scenario, it turns out that the impact on performance is negligible unless the central unit is located at a distance $\geq$20 km from the peripherals. The robustness of the system has been attested confirming the suitability of commercial X-band devices for a shipborne scenario with 200 m-long fibers. Scalability of the number of RPs and bands is possible, with the main limitation given by the available optical power to be divided, eventually expected to impact each signal SNR and therefore, the radar system performance. A numerical analysis in this sense is planned as a forthcoming activity.

Funding. Ministero dell'Università e della Ricerca (FISR2019_03476).

Acknowledgment. The work is partially supported by EU under the Italian National Recovery and Resilience Plan (NRRP) of Next Generation EU, partnership on "Telecommunications of the Future" (PE00000001 – Program "RESTART"), and by the Italian Ministry of University and Research through the COSMOS project (FISR2019_03476)

Disclosures. The authors declare no conflicts of interest.

Data availability. Data underlying the results presented in this paper are not publicly available at this time but may be obtained from the authors upon reasonable request.

Supplemental document. See Supplement 1 for supporting content.

REFERENCES

1. A. Haimovich, R. Blum, and L. Cimini, IEEE Sig. Proc. Mag. **25**, 116 (2008).
2. Q. He, R. S. Blum, H. Godrich, *et al.*, IEEE J. Sel. Top. Signal Process. **4**, 79 (2010).
3. S. Maresca, A. Malacarne, P. Ghelfi, *et al.*, in *IEEE Radar Conference* (2021), p. 1.
4. S. Maresca, F. Scotti, G. Serafino, *et al.*, Opt. Lett. **45**, 3953 (2020).
5. A. Malacarne, S. Maresca, F. Scotti, *et al.*, J. Lightwave Technol. **38**, 6257 (2020).
6. S. Maresca, G. Serafino, C. Noviello, *et al.*, J. Lightwave Technol. **40**, 6626 (2022).
7. J. McKinney, Nature **507**, 310 (2014).
8. G. Serafino, S. Maresca, C. Porzi, *et al.*, IEEE J. Sel. Top. Quantum Electron. **28**, 1 (2022).
9. G. Serafino, S. Maresca, M. M. H. Amir, *et al.*, in 19th European Radar Conference (EuRAD) Milan, Italy (September 28–30, 2022) 1.
10. J. P. Cahill, W. Zhou, and C. R. Menyuk, Appl. Opt. **56**, B18 (2017).
11. L. Duan, Phys. Rev. A **86**, 023817 (2012).
12. J. Taylor, S. Datta, A. Hati, *et al.*, IEEE Photonics J. **3**, 140 (2011).
13. K. Volyanskiy, Y. K. Chembo, L. Larger, *et al.*, J. Lightwave Technol. **28**, 2730 (2010).
14. P. Wan and J. Conradi, J. Lightwave Technol. **14**, 288 (1996).
15. J. P. Cahill, O. Okusaga, W. Zhou, *et al.*, Opt. Express **23**, 6400 (2015).
16. "Guidance Notes General Overview of Ship Structural Vibration Problems," Lloyd's Register, 2021, https://www.lr.org/en/knowledge/lloyds-register-rules/guidance-notes/guidance-notes-general-overview-of-ship-structural-vibration-problems/.
17. J. Taylor, C. Nelson, A. Hati, *et al.*, IEEE International Frequency Control Symposium (2008), p. 807.
18. "Fixed Frequency Synthesizer Surface Mount Module," SFS9280C-LF, Z-Communications, Inc., https://www.zcomm.com/pdfs/datasheets/SFS9280C-LF.pdf.